



Fabrication of CuBi_2O_4 photocathode through novel anodic electrodeposition for solar hydrogen production



Yukihiro Nakabayashi, Masami Nishikawa, Yoshio Nosaka^{*,1}

Department of Materials Science and Technology, Nagaoka University of Technology, Nagaoka, 940-2188 Japan

ARTICLE INFO

Article history:

Received 19 October 2013
Received in revised form 10 January 2014
Accepted 14 January 2014
Available online 28 January 2014

Keywords:

Co-electrodeposition
tartaric acid
photoelectrochemical cell

ABSTRACT

Copper bismuth oxide (CuBi_2O_4) film electrodes were fabricated by anodic co-electrodeposition of Bi_2O_3 and CuO , followed by heat treatment in air at 500°C . The compositions of the electrolyte solution, such as concentrations of Cu^{2+} , Bi^{3+} , and tartaric acid, alkaline strength, and temperature, were optimized to fabricate pure CuBi_2O_4 films on FTO substrates. XRD and optical absorption were employed to confirm the formation of CuBi_2O_4 , and SEM observation showed the fabrication of a closed packed film with good contact to the FTO substrate. Mott-Schottky plots based on Nyquist plots at various potentials gave the flat band potential of 0.62 V (vs. Ag/AgCl) at $\text{pH } 6.0$. Since the band gap energy measured was 1.80 eV , the conduction band bottom locates at -0.98 V (vs. NHE). At the potential more negative than 0 V (vs. Ag/AgCl), the photo cathodic current for hydrogen production was observed under visible light irradiation in a deoxygenated $0.1\text{ M Na}_2\text{SO}_4$ solution. The film electrode sustained the photo electrochemical activity in the electrolyte solution at -0.3 V (vs. Ag/AgCl), at least, for 100 min .

© 2014 Elsevier Ltd. All rights reserved.

1. Introduction

Water splitting with photocatalyst electrodes has been considered as a promising way to convert solar energy into chemical energy of hydrogen. For efficient water splitting, photo electrodes to produce hydrogen or oxygen have been investigated to respond to visible light in solar power spectrum [1]. Photoelectrode to produce hydrogen, i.e., photocathode, has been investigated using conventional photocatalysts [2], however, the absorption edge was confined to UV and near UV light of wavelength shorter than 500 nm ; for example, La-doped NaTaO_3 ($\sim 300\text{ nm}$) [3], SrTiO_3 ($\sim 388\text{ nm}$) [4], TiO_2 ($\sim 410\text{ nm}$) [4], CdS ($\sim 500\text{ nm}$) [5] and TaON ($\sim 500\text{ nm}$) [6]. Copper (I) oxide (Cu_2O) is an exceptional material to exhibit the absorption edge at a longer wavelength ($\sim 620\text{ nm}$) [7]. However, Cu_2O was depleted the photo electrochemical activity due to the reduction of Cu^+ of Cu_2O into Cu^0 under an applied cathodic potential [8,9]. Therefore, we have to explore other photo-electrochemically stable materials being capable of response to visible light of longer wavelength. Copper bismuth oxide (CuBi_2O_4) was chosen in the present study because of the absorption edge at $\sim 800\text{ nm}$ [10–13] and the stable photo electrochemical activity for reduction reaction in alkaline solution has been reported [12].

For fabrication of CuBi_2O_4 films on substrates, electrodeposition was a low-cost technique for large area films. Additionally,

the electrodeposited film could exhibit good contact to the substrate [7]. In a previous report, CuBi_2O_4 films were fabricated by co-electrodeposition of metallic copper (Cu) and bismuth (Bi) on a FTO (F-doped tin oxide) substrate, followed by heat-treatment to change them into metal oxides [12]. However, according to the report, the CuBi_2O_4 film on the FTO substrate was very fragile [12]. It was considered that the oxidation process of the deposited metals weaken the contact of the films to the substrates. Therefore, electrodeposition with the state of metal oxides would be desired because the charge of metals in metal oxides would not be changed before and after the heat-treatment. As for the electrodeposition of metal oxide, anodic oxidation in alkaline solutions containing Cu^{2+} or Bi^{3+} with a chelating reagent has been reported so far for CuO [14] and Bi_2O_3 [15], respectively. Our approach in the present work was co-electrodeposition of CuO and Bi_2O_3 by anodic electrolysis in a solution containing both Cu^{2+} and Bi^{3+} ions with tartaric acid for fabricating CuBi_2O_4 films on FTO substrates, followed by heat-treatment in air. To yield the pure CuBi_2O_4 films, we adjusted the conditions for electrodeposition; alkalinity (pH), temperature and composition of electrolyte solution and the electrode potential. Finally, in the present study we succeeded to fabricate pure CuBi_2O_4 film electrodes with a definite photo electrochemical response.

2. Experimental

2.1. Chemical reagents

Bismuth(III) nitrate pentahydrate ($\text{Bi}(\text{NO}_3)_3 \cdot 5\text{H}_2\text{O}$), copper(II) sulfate pentahydrate ($\text{CuSO}_4 \cdot 5\text{H}_2\text{O}$), tartaric acid, sodium sulfate

* Corresponding author.

E-mail address: nosaka@nagaokaut.ac.jp (Y. Nosaka).

¹ ISE member

(Na_2SO_4), and sodium hydroxide (NaOH) were purchased from Nacalai Tesque Inc. and used without further purification. Electrolyte solutions for electrodeposition and photoelectrochemical evaluation were prepared with pure water treated with a Milli-Q system.

2.2. Fabrication of CuBi_2O_4 film electrode

The CuBi_2O_4 films were fabricated by two steps; electrodeposition of the precursor of CuBi_2O_4 on an FTO substrate and the heat treatment in air.

The electrodeposition was carried out by three electrode system in a homemade electrochemical cell shown in Fig. 1. The working electrode was a FTO substrate (AGC Fabritec, Inc.), and the reference electrode was an Ag/AgCl electrode (BAS, Inc., Type RE-1 C). The counter electrode was a platinum (Pt) coil, which was separated from the FTO substrate by an ion exchange membrane (Aldrich Science, Nafion[®] 117) and contained in a 0.1 M ($M = \text{mol dm}^{-3}$) Na_2SO_4 solution of pH 13.0 adjusted by NaOH. All FTO substrates were rinsed with a detergent and pure water, and then connected to a lead wire by soldering. The area of the FTO substrate was regulated into 1 cm × 1 cm by epoxy adhesive. Just before the electrochemical deposition, the surface of the FTO substrate was activated under air plasma in Mini Sputter (Anelva, Inc., SPM112) until the formation of hydrophilic surface checked by dropping pure water on it. The three electrodes were connected to a potentiostat (Princeton Applied Research, VersaSTAT3) for electrodeposition. The electrolyte solution in the homemade cell was heated at 65 °C in hot water and the temperature was monitored by a glass thermometer. The solution was prepared by dissolving $\text{Bi}(\text{NO}_3)_3$, CuSO_4 , tartaric acid, and 0.1 M Na_2SO_4 , and then adjusted at pH 13.0 by NaOH. Electrodeposition was carried out in this electrolyte solution at 65 °C by applying anodic potential. After electrodeposition, the precursor film on the FTO substrate was carefully rinsed with pure water.

The precursor film was heated at 500 °C in air for 4 h to fabricate a sample film.

2.3. Evaluation of CuBi_2O_4 film electrode

To examine crystal phase of the samples, X-ray diffraction (XRD) patterns were recorded with a diffractometer (Mac Science Co., MO3X HF) using a Cu K α source. For the calculation of the lattice parameters, a software (Cell Calc, Ver.2.20) [16] was employed. To examine the atomic component of the samples, X-ray photo

electron spectroscopy (XPS) was employed with a spectrometer (JEOL, JPS-9010TR) using a monochromatic Mg K α source. The ratios of the elements on the surface were estimated, by using the peak areas of Cu 2p_{3/2} and Bi 4f_{7/2} with the values of relative sensitivity of the instrument.

Transmittance and reflectance of the sample film were measured with an optical spectrophotometer (Shimadzu, UV3150) equipped with an integrating sphere, using BaSO_4 powder as a reference for reflectance. The absorbance was calculated from the transmittance and corrected with the reflectance. The photo absorption property could be examined by eq. (1), [17–19]

$$\{(\text{Abs.})(h\nu)\}^{(1/n)} = (\text{Constant})(h\nu - E_g) \quad (1)$$

The superscript (n) in the equation was dependent on the transition type of semiconductors. This relationship is originally based on the absorption coefficient (α) instead of the absorbance (Abs.). However the Abs. for the thin film can be calculated to be $0.4343\alpha\ell$ with the light-path-length ℓ or effective film thickness. Therefore, eq. (1) is applicable to estimate the band gap energy E_g from the plot of the left term against photon energy, $h\nu$.

Photo electrochemical properties of the CuBi_2O_4 film electrode were evaluated by a three electrode system in a 0.1 M Na_2SO_4 aqueous solution with a potentiostat (Hokuto Denko, HSV100), where the reference electrode was an Ag/AgCl electrode (BAS, Inc., RE-1 C) and the counter electrode was a Pt coil in 0.1 M Na_2SO_4 aqueous solution (pH 6) separated by ion exchange membrane (Aldrich Science, Nafion[®] 117). The potentiostat (Princeton Applied Research, VersaSTAT3) was employed for the measurement of the electrochemical impedance of the CuBi_2O_4 film electrode. When we measured electrochemical impedance, ion exchange membrane was not employed.

For deoxygenated condition, the dissolved oxygen (DO) in the solution was diminished by bubbling nitrogen (N_2) for 1 h, and DO concentration measured by a DO meter (Mettler Toledo Inc., MO128) was less than 0.03 mgL⁻¹. A 500 W xenon arc lamp (Ushio Inc., UXL500SX) was employed as an incident light source for photo current, and the wavelength was regulated by a sharp cut filter (Sigma Koki Co., Ltd, SCF50S42L) into the range of $\lambda \geq 420$ nm.

For the measurements of incident photon to current efficiency (IPCE) [12], current-time (I-t) curves at a constant potential were recorded for the monochromatic lights of the 500 W xenon arc lamp and the steady state current was employed. The wavelength was checked by a spectrometer (Avantes Co., AvaSpec2048USB) and the

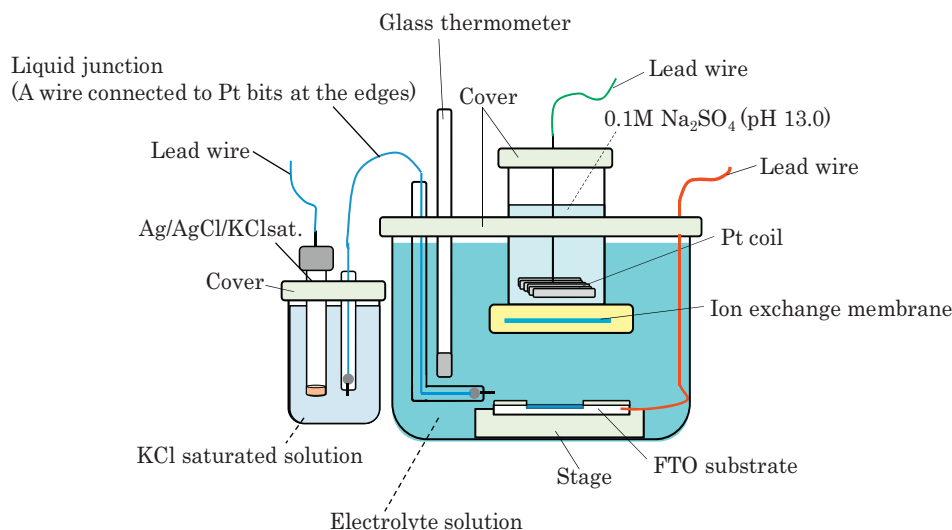


Fig. 1. The illustration of the homemade cell for electro deposition.

light intensity was measured by an optical power meter (Advantest Co., TQ8210). The IPCE at each wavelength (λ) was calculated by the following equation.

$$\text{IPCE}(\lambda) = \left(\frac{\text{Number of photocurrent electrons}(\lambda)}{\text{Number of incident photons}(\lambda)} \right) \times 100(\%) \quad (2)$$

The number of photocurrent electrons ($s^{-1} \text{cm}^{-2}$) was calculated from the photo current density of the steady state (μAcm^{-2}), while the number of incident photons ($s^{-1} \text{cm}^{-2}$) was calculated from the intensity of incident light (μWcm^{-2}) at each λ .

3. Results and discussion

3.1. Effect of chelating reagent

In literatures, electrochemical film fabrication of Bi_2O_3 and CuO have been carried out by anodic electrolysis in alkaline solutions containing metal ions; the condition for Bi_2O_3 was $\text{pH} \sim 14.0$ at 65°C [15] and the condition for CuO was $\text{pH} \sim 13.0$ at 30°C [14]. For co-electrodeposition of Bi_2O_3 and CuO , the temperature and pH of the electrolyte solution was chosen to be 65°C and $\text{pH} 13.0$, respectively, because electrodeposition could proceed efficiently at high temperature [20] and CuO would be unstable in quite strong alkaline solutions as shown in the Pourbex diagram of Cu -water system [21].

To determine the suitable electrode potential for electrodeposition, we examined a current-voltage (I - V) property under several conditions. Fig. 2(A) shows the I - V property with an FTO electrode for the solution containing 0.07 M Bi^{3+} , 0.03 M Cu^{2+} , $0.13 \text{ M tartaric acid}$, and $0.1 \text{ M Na}_2\text{SO}_4$. The concentration of tartaric acid for this metal ion component was determined from a test experiment, in which a precipitate was generated when the concentration of tartaric acid was below 0.12 M . The I - V curve exhibited three anodic currents, (1), (2) and (3), having the onset at 1.0 V , 1.8 V , and 2.2 V (vs. Ag/AgCl), respectively. The current (3) is attributable to the oxidation of water, considering the literature, in which the anodic current generated in electrolyte solution of $\text{pH} 13.0$ did not show the saturation of current by applying a potential difference of 0.4 V from the onset potential [22]. Therefore, we chose 2.2 V as the deposition potential, which correspond to the onset potential of water. At this applied potential, the anodic currents of (1) and (2) were large, on the other hand, the anodic current of (3) was negligible. Even when oxygen was produced, the rate was slow enough to be dissolved in the electrolyte solution and not to leave bubbles on the electrode surface.

As shown later, the crystal phases of CuBi_2O_4 and Bi_2O_3 were observed after the film deposited under the condition of Fig. 2(A)

Table 1

The compositions of the solutions with $0.1 \text{ M Na}_2\text{SO}_4$ at $\text{pH} 13.0$ for fabrication of the samples for XRD analysis.

Electrolyte solution	Cu^{2+}/M	Bi^{3+}/M	Tartaric acid/ M
A	0.03	0.07	0.13
B	0.03	0.03	0.06
C	0.03	0.02	0.05

was heat treatment in air at 500°C for 4 h. Therefore, either Cu^{2+} or Bi^{3+} would be deposited on the FTO substrate by an electrochemical reaction for the anodic current (1) and the other metal ion would be deposited by the electrochemical reaction for the anodic current (2). However, we could not precisely identify the reaction for the anodic currents (1) and (2). Anyway, the suitable potential for electrodeposition was determined to be 2.2 V (vs. Ag/AgCl) for preparing the precursor of CuBi_2O_4 .

As the first step, we examined the effect of the concentration of tartaric acid on the anodic currents of (1) and (2) in Fig. 2(A), where the concentration was adjusted to sustain the solution without precipitation of metal oxide (or hydroxide). When the concentration of tartaric acid was increased to 0.224 M , the I - V curve of Fig. 2(A) was changed into that of Fig. 2(B). Compared with the I - V curve of Fig. 2(A), the anodic current of (1) was increased, while the anodic current of (2) was decreased. Therefore, the extra concentration of tartaric acid accelerated the electrochemical reaction for the anodic current of (1) and decelerated the electrochemical reaction for the anodic current of (2). Thus, the concentration of tartaric acid dominated the electrochemical reactions likewise to the concentration of metal ions. The effect of extra concentration of tartaric acid was realized when only the concentration of Bi^{3+} was decreased in order to diminish the Bi_2O_3 from the fabricated electrodes. Therefore, the concentration of tartaric acid was minimized to sustain metal ions in the solution without precipitation at $\text{pH} 13.0$.

3.2. Concentration ratio for Bi^{3+} to Cu^{2+}

The as-deposited film, which was transformed into the composite of CuBi_2O_4 and Bi_2O_3 , would be due to the excess electrodeposition of Bi^{3+} compared to Cu^{2+} . To eliminate the Bi_2O_3 , we adjusted the composition of the solution. Namely, the concentration of Bi^{3+} and tartaric acid were diluted from 0.07 M (solution A) to 0.02 M (solution C), while the concentration of Cu^{2+} was fixed at 0.03 M . The concentration of tartaric acid for each solution was shown in Table 1. We fabricated samples by anodic electrolysis at 2.2 V (vs. Ag/AgCl) for 1 h followed by heat-treatment at 500°C for 4 h.

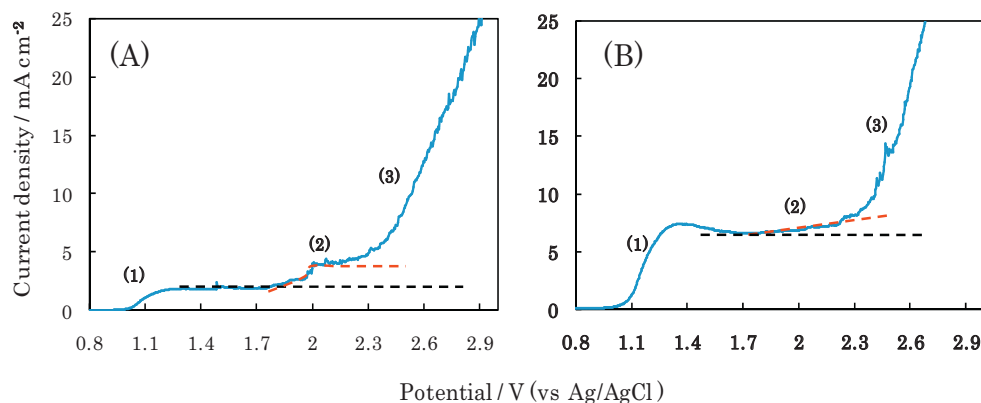


Fig. 2. The effect of the concentration of tartaric acid, (A) 0.13 M or (B) 0.224 M , on the I - V properties. The electrolyte solutions of $\text{pH} 13.0$ at 65°C contained 0.07 M Bi^{3+} , 0.03 M Cu^{2+} , and $0.1 \text{ M Na}_2\text{SO}_4$, in addition to tartaric acid.

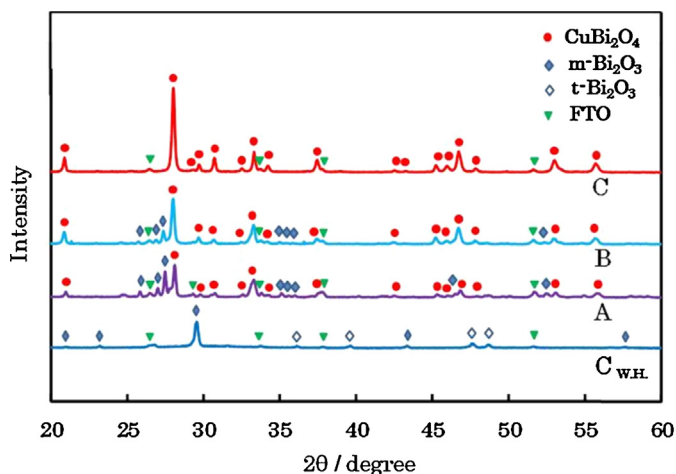


Fig. 3. XRD patterns of the samples fabricated with the electrolyte solutions, A, B, and C, listed in Table 1. At the bottom, $C_{w.H.}$ shows the pattern of the precursor film for the sample C without heat-treatment. m- and t- for Bi_2O_3 represent monoclinic and tetragonal, respectively.

Fig. 3 shows the XRD patterns of the samples obtained for the solution composition in Table 1. The samples for A and B exhibited the XRD peaks of tetragonal CuBi_2O_4 (ICDD, # 00-042-0334) and monoclinic Bi_2O_3 (ICDD, # 00-041-1449) crystals, respectively, with the peaks of FTO substrate. The intensities of the peaks of Bi_2O_3 became weak with the decrease of the Bi^{3+} concentration in the solution. Then, for the sample C, only the peaks of CuBi_2O_4 crystal were observed in the XRD pattern, and no peaks of Bi_2O_3 was observed. Namely, since the heat-treatment caused CuBi_2O_4 alone, the precursor film contained Cu^{2+} and Bi^{3+} at the ratio of 1:2 in the bulk, even though it was co-electrodeposited from the solution of $\text{Cu}^{2+}:\text{Bi}^{3+} = 3:2$. Thus, pure CuBi_2O_4 film without production of Bi_2O_3 was obtained after the heat treatment.

For the pure CuBi_2O_4 film, the lattice parameters were $a = 8.4947 \text{ \AA}$ and $c = 5.7943 \text{ \AA}$, which was similar to those ($a = 8.4996 \text{ \AA}$ and $c = 5.8172 \text{ \AA}$) of the tetragonal CuBi_2O_4 . Judging from the XRD patterns, the quality of the CuBi_2O_4 crystal prepared in the present study was as same as that prepared by the high temperature calcination of mixed powders. Therefore, we employed the electrolyte solution C to fabricate pure CuBi_2O_4 films on FTO substrates.

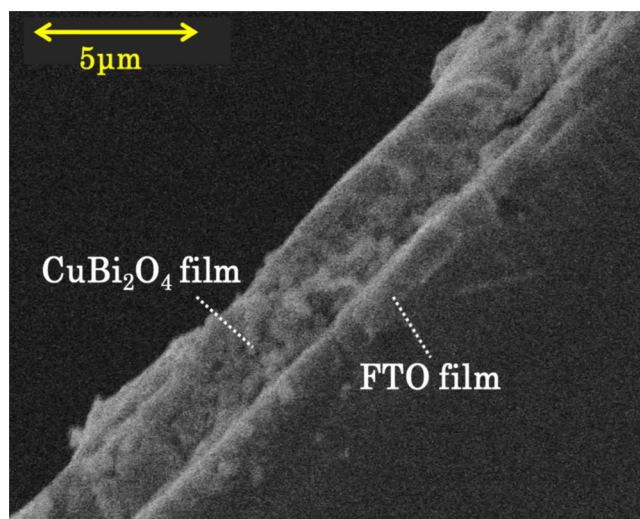


Fig. 5. The SEM image of the cross sectional view of a pure CuBi_2O_4 film electrode fabricated through electrodeposition for 20 min.

Next, we explored the precursor film for pure CuBi_2O_4 . The XRD pattern of the precursor film before heat treatment was exhibited at the bottom in Fig. 3. Unfortunately, XRD pattern of the as-deposited film did not show the peaks of CuBi_2O_4 crystal. The peaks indicated the formation of monoclinic (ICDD, # 01-080-2589) and tetragonal (ICDD, # 01-073-6885) crystalline Bi_2O_3 . The growth of monoclinic crystalline Bi_2O_3 would be influenced by organic species such as tartaric acid during electrodeposition, leading to different growth from those after heat-treatment [13]. On the other hand, the crystalline CuO was not observed.

Thus, the Cu^{2+} and Bi^{3+} ions were electrodeposited as a composite of amorphous CuO and crystalline Bi_2O_3 , and they were combined into CuBi_2O_4 by solid phase reaction [11,23] at 500°C .

To explore the state of metal ions, we measured XPS charts for the precursor films obtained by electrodeposition for 20 min and the pure CuBi_2O_4 film obtained by the succeeded heat-treatment. Fig. 4(A) shows the XPS charts for the Cu part for the precursor film and the CuBi_2O_4 film. The peaks of Cu $2p_{3/2}$ for both of them were located at 933.7 eV and were assigned to CuO [24]. It suggested that Cu^{2+} binding to oxygen existed in the precursor film and the CuBi_2O_4 film. The CuO was electrodeposited as amorphous phase,

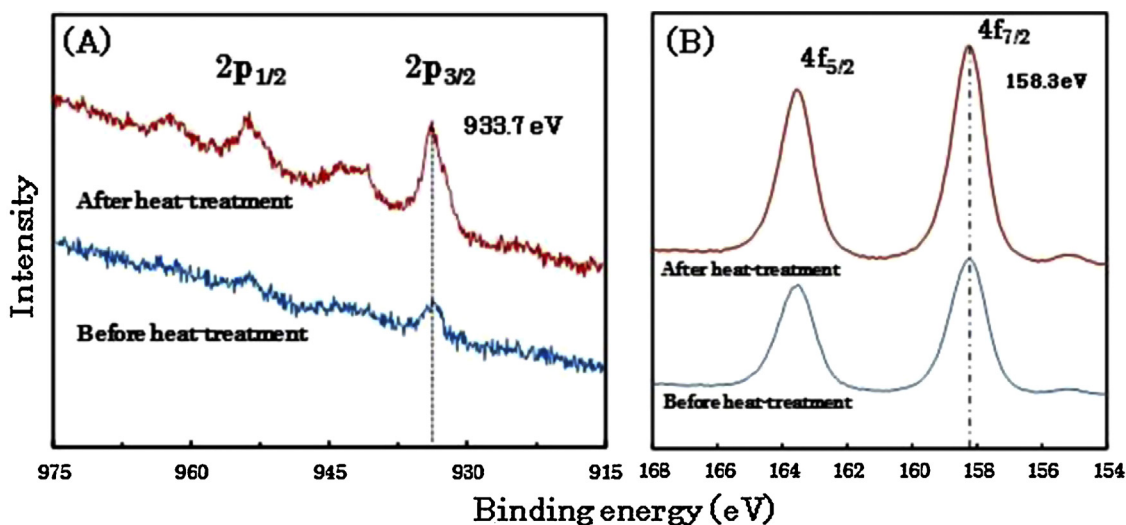


Fig. 4. The XPS charts of (A) Cu and (B) Bi part for a precursor film Before (blue line) and after (red line) the heat-treatment for pure CuBi_2O_4 film fabricated through electrodeposition for 20 min.

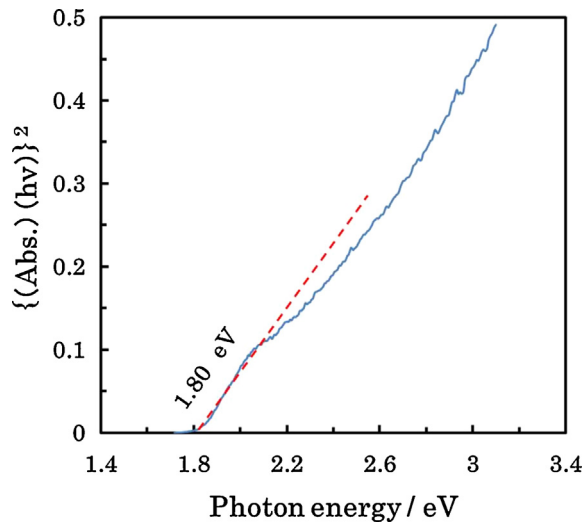


Fig. 6. The threshold energy of direct transition of CuBi_2O_4 .

because there are no peaks of crystalline CuO in the XRD pattern of the precursor film. Fig. 4(B) shows the XPS charts for the Bi part for the precursor film and the CuBi_2O_4 film. The peaks of $\text{Bi } 4f_{7/2}$ for both of them were located at 158.3 eV and were assigned to Bi_2O_3 [25], suggesting that Bi^{3+} binding to oxygen existed in the precursor film and the CuBi_2O_4 film. As for the precursor film, it was coincident with the interpretation of the XRD pattern at the bottom of Fig. 3.

The ratio of Cu^{2+} to Bi^{3+} on the surface of the precursor film was 1:3.7 and it became 1:3.9 after heat treatment, suggesting that heat-treatment hardly influenced on the ratio of Cu^{2+} and Bi^{3+} . However, the value was different from the ratio of Cu^{2+} to Bi^{3+} of pure CuBi_2O_4 (1:2) in the bulk. This difference may be caused by the dissolution of CuO from the surface of as-deposited film in the period from finishing electrodeposition to rinsing the deposited precursor.

3.3. Characterization of the film

To examine the morphology of the pure CuBi_2O_4 film, SEM observation was employed. Fig. 5 shows the SEM image of cross sectional view obtained for a CuBi_2O_4 film electrode.

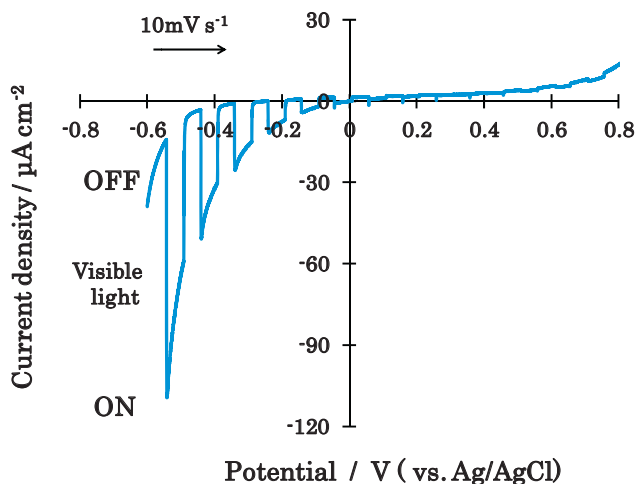


Fig. 7. The I-V property of the CuBi_2O_4 film electrode in deoxygenated 0.1 M Na_2SO_4 solution (pH 6).

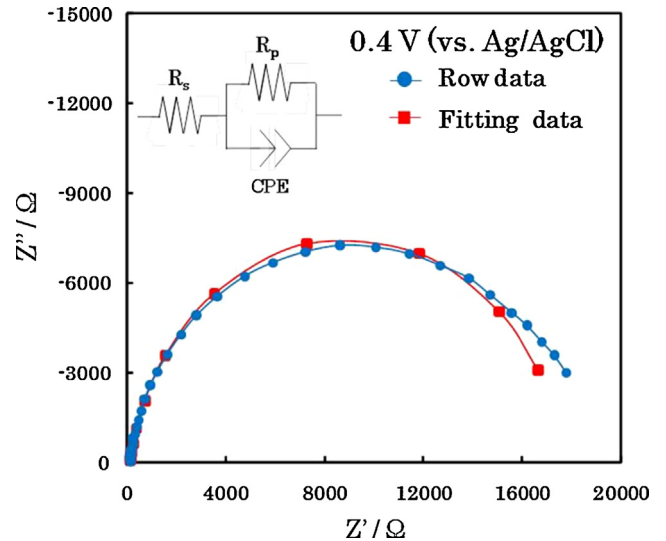


Fig. 8. Nyquist plot of the pure CuBi_2O_4 film electrode in a deoxygenated 0.1 M Na_2SO_4 solution (pH 6).

In the SEM image, the pure CuBi_2O_4 film of 3- μm thickness was fabricated through electrodeposition for 20 min. As far as the SEM images showed, the CuBi_2O_4 film was closed packed and no crevice appeared between the film and the FTO substrate. Additionally, the pure CuBi_2O_4 film was mechanically tough because it was not peeled out from the FTO substrate by rubbing with soft paper strongly.

To elucidate photo absorption property, the relationship of eq.(1) for direct transition ($n=0.5$) was applied and shown in Fig. 6. The figure shows a linear correlation near the intercept to the axis of photon energy. Therefore, the direct transition was suggested for CuBi_2O_4 . From the intercept to the axis of photon energy, we evaluated the band gap energy to be 1.80 eV, which is in good agreement with the reported values of 1.5 to 1.8 eV [10–13].

3.4. Photoelectrochemical evaluation

The electrochemical properties were examined for the pure CuBi_2O_4 film electrode fabricated through electrodeposition for 20 min.

Fig. 7 shows the I-V property for the CuBi_2O_4 film electrode, where the electrode potential was scanned from -0.6 V to 0.8 V at

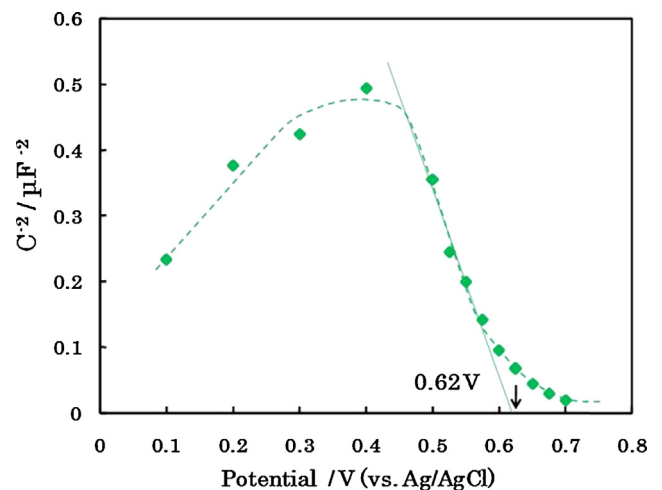


Fig. 9. The Mott-Schottky plot of the pure CuBi_2O_4 film electrode in a deoxygenated 0.1 M Na_2SO_4 solution (pH 6).

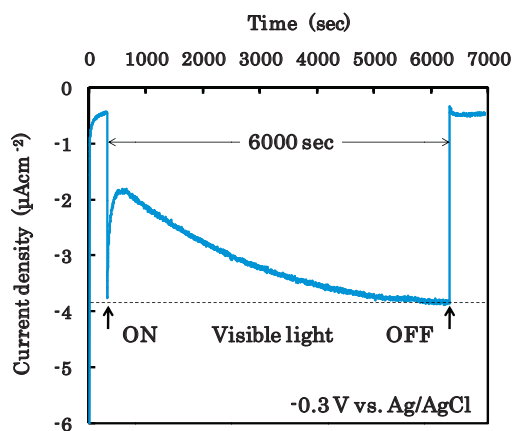


Fig. 10. The I-t property of the CuBi_2O_4 film electrode in a deoxygenated 0.1 M Na_2SO_4 solution (pH 6).

the scan rate of 10 mV s^{-1} . During the scan, the visible light was irradiated intermittently at 5-sec interval.

Photocathodic current was generated at the potential more negative than 0 V under visible light irradiation. The observation of photocathodic current indicates the reduction of some species in the solution by the photo excited electrons at the CuBi_2O_4 film electrode. In the deoxygenated condition, proton of water is the most probable candidate to be reduced.

To confirm the activity for water reduction to produce hydrogen, the band position was estimated by the Mott-Schottky plot of the CuBi_2O_4 film electrode fabricated in our study. To prepare the plot, the electrochemical impedance was measured for the electrode at various applied potentials. Fig. 8 demonstrates an example of the Nyquist plot of the electrode in the deoxygenated 0.1 M Na_2SO_4 aqueous solution (pH 6) at 0.4 V (vs. Ag/AgCl) at the frequency from 1 to 10000 Hz. We estimated the value of capacitance in the CuBi_2O_4 film by fitting the plot to the equivalent circuit in Fig. 8, where R_s is the total resistance of the electrolyte solution and the CuBi_2O_4 film, R_p is the resistance of electrochemical reaction, and then CPE is constant phase element. In this study, it was considered that the CPE constant was equivalent to the capacitance in the CuBi_2O_4 film. The values of the capacitance were estimated in the potential range from 0.1 to 0.7 V.

Fig. 9 shows the Mott-Schottky plot of (capacitance) $^{-2}$ vs. potential. A linear correlation, which was similar to those of conventional p-type semiconductors (Cu_2O , CuO and GaN) [18,26], was shown in the plot. It suggested that CuBi_2O_4 was also a p-type semiconductor. The extrapolation on the linear portion to the axis of potentials and the slope value gave the flat band potential, E_{FB} , and the acceptor density, N_A , respectively. The values of E_{FB} and N_A were 0.62 V (vs. Ag/AgCl) and $5.67 \times 10^{17} \text{ cm}^{-3}$, respectively, assuming that the dielectric constant of CuBi_2O_4 was 100 obtained under 290 K at 10000 Hz [27]. The position of E_{FB} is close to the top of valance band, E_{VB} , for p-type semiconductors. We could estimate approximately that the E_{FB} was equal to the potential of the E_{VB} , that is, $E_{\text{FB}} \approx E_{\text{VB}}$. Also, we could estimate that the position of conduction band bottom, E_{CB} , was at -1.18 V (vs. Ag/AgCl) or -0.98 V (vs. NHE), considering the E_g of 1.80 eV. It is more negative than the reduction potential for proton of water to produce hydrogen under pH 6 at -0.553 V (vs. Ag/AgCl). Therefore, it is assured that CuBi_2O_4 has an activity for water reduction.

The stable photo electrochemical performance was examined by long term electrolysis in a deoxygenated 0.1 M Na_2SO_4 aqueous solution at -0.3 V (vs. Ag/AgCl) shown in Fig. 10. The cathodic current was increased just after starting visible light irradiation and it was decreased promptly. The current spike could be attributed to a transitional electron trapping on the electrode surface followed by a charge recombination. The cathodic current was increased gradually and reached in a steady state within 80 min after starting light irradiation. Just after stopping light irradiation, the cathodic current was decreased promptly and reached constant. Therefore, the increase of the cathodic current under light irradiation was not attributed to the increase of dark current but to the increase of photocurrent. It is considered that during photo electrolysis in the electrolyte solution, some species was generated on the surface of the electrode to promote the photocathodic reaction until the surface was occupied fully by it.

Fig. 11 shows the XPS charts for the CuBi_2O_4 film before and after long term photo electrolysis shown in Fig. 10. The peak of Cu $2p_{3/2}$ shown in Fig. 11(A) was shifted from 933.7 eV to 932.0 eV, suggesting that the chemical state of Cu^{2+} was changed to Cu^0 [24]. While, the peak of Bi $4f_{7/2}$ shown in Fig. 11(B) remained at 158.3 eV, suggesting the chemical state of Bi^{3+} was not changed. On the other hand, the ratio of Cu^{2+} to Bi^{3+} became 1:1, suggesting that, during the photo electrolysis, Bi^{3+} at the surface was dissolved selectively into the electrolyte solution and Cu^{2+} stayed on the

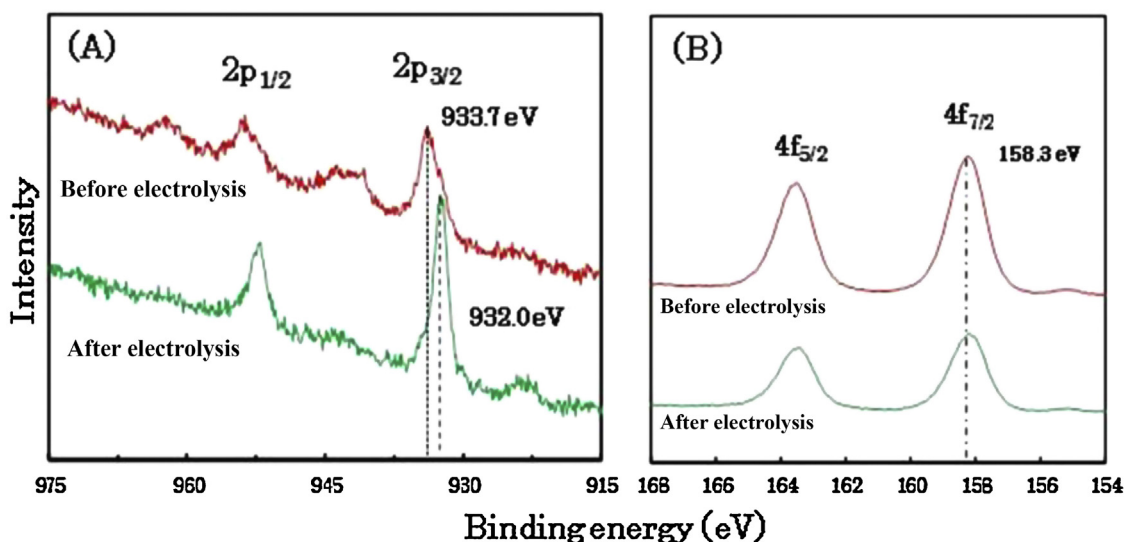


Fig. 11. The XPS charts for (A) Cu part and (B) Bi part of the CuBi_2O_4 film electrodes before (red line) and after (green line) long term photo electrolysis shown in Fig. 10.

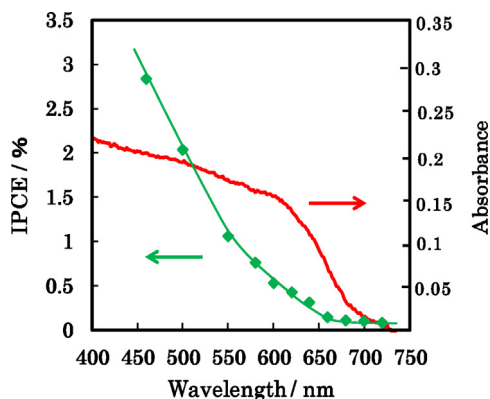


Fig. 12. The IPCE and the absorbance of a CuBi_2O_4 film electrode: the IPCE was calculated with steady state photocathodic current at -0.3 V (vs. Ag/AgCl) in a deoxygenated $0.1\text{ M Na}_2\text{SO}_4$ solution (pH 6).

CuBi_2O_4 film surface as Cu. This Cu could act as a co-catalyst to separate the photo excited electron-hole pair on the surface of the film electrodes, leading to the gradually increase of the photocathodic current shown in Fig. 10.

The photo electro chemical activity remained, at least, within 100 min. It was reported that a Cu_2O film electrode depleted the photo electrochemical activity within 20 min under photo electrolysis in N_2 purged $1\text{ M Na}_2\text{SO}_4$ aqueous solution [9]. Therefore, compared with Cu_2O film electrode, the CuBi_2O_4 film electrode of our study exhibited more stable photo electrochemical activity.

Fig. 12 shows the IPCE and the absorption spectrum for a CuBi_2O_4 film electrode. For the absorption spectrum, photo absorption edge was located at 689 nm and the absorbance increased toward shorter wavelength. However, for IPCE, the onset of IPCE was 650 nm and increased gradually toward short wavelength. And the IPCE was small even in short wavelength (less than 3%).

The dependence of IPCE on wavelength and small IPCE would be derived from a charge recombination leading to loss of photo excited carrier [2]. The excited electrons, which are generated by the incident light around 689 nm, would hardly contribute to the reduction reaction due to a rapid charge recombination. As the wave length of incident light became short, the charge recombination became suppressed by the excess energy for inter-band transition, leading the dependence of IPCE on the wavelength as shown in Fig. 12.

Compared with the CuBi_2O_4 film electrode fabricated through co-electro deposition of Bi and Cu metals [12], our CuBi_2O_4 film electrode shows larger IPCE values under similar experimental conditions. For example, our electrode exhibited 7.5 times larger IPCE value at 580 nm. This would be due to the tight contact of our CuBi_2O_4 films to FTO substrates as shown in the cross sectional view of Fig. 5.

4. Conclusions

In the present study, pure CuBi_2O_4 films were successfully fabricated on FTO substrates by anodic electrodeposition in the adjusted electrolyte solution containing Bi^{3+} , Cu^{2+} , and tartaric acid, followed by heat-treatment in air. Although as-deposited films consisted of crystalline Bi_2O_3 and amorphous CuO , the CuBi_2O_4 film obtained by the heat-treatment at 500°C exhibited mechanical toughness and good contact to the FTO substrate.

Under visible light irradiation, the CuBi_2O_4 film electrode generated photo cathodic current at the potential more negative than 0 V (vs. Ag/AgCl) in a deoxygenated $0.1\text{ M Na}_2\text{SO}_4$ solution (pH 6). The electrode sustained the photo electrochemical activity in the photo electrolysis at -0.3 V for 100 min. It was

expected that the film electrode could perform hydrogen production under solar light irradiation, considering the E_{cb} of -0.98 V (vs. NHE) for CuBi_2O_4 deduced from Mott-Schottky plot and bandgap energy.

The IPCE value was less than 3% in the range of 450–689 nm. Possible significant charge recombination leads to the decrease of IPCE, especially in longer wavelength. To improve the efficiency of photocathodic current, it will be required that the factors of the charge recombination be disclosed by selecting the fabrication conditions.

The procedure developed in the present study to adjust the components of electrolyte solution and other conditions could open the way to fabricate a variety of mixed metal oxides through electrodeposition technique.

References

- [1] M.G. Walter, E.L. Warren, J.R. McKone, S.W. Boettcher, Q. Mi, E.A. Santori, N.S. Lewis, *Solar Water Splitting Cells*, *Chem. Rev.* 110 (2010) 6446–6473.
- [2] X. Chen, S. Shen, L. Guo, S.S. Mao, *Semiconductor-based Photocatalytic Hydrogen Generation*, *Chem. Rev.* 110 (2010) 6503–6570.
- [3] A. Iwase, H. Kato, A. Kudo, The effect of Au cocatalyst loaded on La-doped NaTaO_3 on photocatalytic water splitting and O_2 photoreduction, *Appl. Catal. B: Environ.* 136–137 (2013) 89–93.
- [4] R.B. Gupta (Ed.), *Hydrogen Fuel Production, Transport and Storage*, CRC Press Taylor and Francis, 2009, p. 234, Chap. 7.
- [5] F. Liu, Y. Lai, J. Liu, B. Wang, S. Kuang, Z. Zhang, J. Li, Y. Liu, Characterization of chemical bath deposited CdS thin films at different deposition temperature, *J. Alloy. Compounds* 493 (2010) 305–308.
- [6] R. Abe, M. Higashi, K. Domen, Facile Fabrication of an Efficient Oxynitride TaON Photoanode for Overall Water Splitting into H_2 and O_2 under Visible Light Irradiation, *J. Am. Chem. Soc.* 132 (2010) 11828–11829.
- [7] P. Chatchai, A. Nosaka, Y. Nosaka, The Effect of Platinum Deposition on the Water Photo-Reduction at p- Cu_2O Semiconductor Electrodes with Visible Light Irradiation, *Electrochemistry* 79 (2011) 821–825.
- [8] F. Caballero-Briones, J.M. Artes, I. Diez-Perez, P. Gorostiza, F. Sanz, Direct Observation of the Valence Band Edge by in Situ ECSTM-ECTS in p-Type Cu_2O Layers Prepared by Copper Anodization, *J. Phys. Chem. C* 113 (2009) 1028–1036.
- [9] A. Paracchino, V. Laporte, K. Sivula, M. Gratzel, E. Thimsen, Highly active oxide photocathode for photoelectrochemical water reduction, *Nature Mat.* 10 (2011) 456–461.
- [10] T. Arai, M. Yanagida, Y. Konishi, Y. Iwasaki, H. Sugihara, K. Sayama, Efficient Complete Oxidation of Acetaldehyde into CO_2 over $\text{CuBi}_2\text{O}_4/\text{WO}_3$ Composite Photocatalyst under Visible and UV Light Irradiation, *J. Phys. Chem. C* 111 (2007) 7574–7577.
- [11] K. Yamada, K. Yamamoto, T. Sonoda, H. Yamane, S. Matsushima, H. Nakamura, Visible Light Activity of Photocatalytic Composites Composed of Metal Oxides, *Nanosci. Nanotechnol. Lett.* 4 (2012) 712–715.
- [12] H. Nathan, V.C. Holmberg, B.A. Korgel, C.B. Mullins, Electrochemical Synthesis and Characterization of p- CuBi_2O_4 Thin Film Photocathodes, *J. Phys. Chem. C* 116 (2012) 6459.
- [13] A.M. Abdulkarem, J. Li, A.A. Aref, L. Ren, E.M. Elssfah, H. Wang, Y. Ge, Y. Yu, CuBi_2O_4 single crystal nanorods prepared by hydrothermal method: Growth mechanism and optical properties, *Mat. Res. Bull.* 46 (2011) 1443.
- [14] S. Joseph, P.V. Kamath, S. Upadilya, Electrochemical Synthesis of Oriented CuO Coatings on Stainless Steel Substrates: Solution-Mediated Control over Orientation, *J. Electrochem. Soc.* 156 (2009) E18–E20.
- [15] K. Laurent, G. Y. Wang, S. Tusseau-Nenez, Y. Leprince-Wang, Structure and conductivity studies of electrodeposited ($-\text{Bi}_2\text{O}_3$ Solid State Ionics 178 (2008) 1735–1739.
- [16] <http://homepage2.nifty.com/~hsc/soft/cellcalc.html>.
- [17] S.U.M. Khan, J. Akikusa, Photoelectrochemical Splitting of Water at Nanocrystalline n- Fe_2O_3 Thin-Film Electrodes, *J. Phys. Chem. B* 103 (1999) 7184.
- [18] K. Nakaoka, J. Ueyama, K. Ogura, Photoelectrochemical Behavior of Electrodeposited CuO , and Cu_2O Thin Films on Conducting Substrates, *J. Electrochem. Soc.* 151 (2004) C661–C665.
- [19] S.M. Pawar, B.S. Pawar, A.V. Moholkar, D.S. Choi, J.H. Yun, J.H. Moon, S.S. Kolekar, J.H. Kim, Single step electrosynthesis of $\text{Cu}_2\text{ZnSnS}_2$ (CZTS) thin films for solar cell application, *Electrochim. Acta* 55 (2010) 4057.
- [20] V. Dhasekaran, T. Mahalingam, R. Chandramohan, J.-K. Rhee, J.P. Chu, Electrochemical deposition and characterization of cupric oxide thin films, *Thin. Solid. Film* 520 (2012) 6608–6613.
- [21] National Institute of Advanced Industrial Science and Technology, Atlas of Eh-pH diagrams. General survey of Japan Open File Report No. 419, May 2005, p47 Bi_2O_3 , p86 CuO .
- [22] Boon Siang Yeo, T. Bel Alexis, Enhanced Activity of Gold-Supported Cobalt Oxide for the Electrochemical Evolution of Oxygen, *J. Am. Chem. Soc.* 133 (2011) 5587–5593.
- [23] E. Abdelkader, L. Nadjia, B. Ahmed, Synthesis, characterization and UV-A light photocatalytic activity of 20 wt% $\text{SrO}-\text{CuBi}_2\text{O}_4$ composite, *Appl. Surf. Sci.* 258 (2012) 5010–5024.

- [24] M.C. Biesinger, L.W.M. Lau, A.R. Gerson, R. StC. Smart, Resolving surface chemical states in XPS analysis of first row transition metals, oxides and hydroxides: Sc, Ti, V, Cu and Zn, *Appl. Surf. Sci.* 257 (2010) 887.
- [25] S.H. Hsieh, G.J. Lee, S.H. Davies, S.J. Masten, J.J. Wu, Synthesis of Cr_2O_3 and Pt doped $\text{RuO}_2/\text{Bi}_2\text{O}_3$ Photocatalysts for Hydrogen Production from Water Splitting, *Am. J. Environ. Eng.* 3 (2013) 115–120.
- [26] K. Fujii, K. Ohkawa, Photoelectrochemical Properties of p-Type GaN in Comparison with n-Type GaN, *Jpn. J. Appl. Phys.* 44 (2005) L909–L911.
- [27] K. Yoshii, T. Fukuda, H. Akahama, J. Kano, T. Kambe, N. Ikeda, Magnetic and dielectric study of Bi_2CuO_4 , *Physica C* 471 (2011) 766–769.